Arsenene: Two-dimensional buckled and puckered honeycomb arsenic systems

C. Kamal[1,*] and Motohiko Ezawa[2,†]

[1]*Indus Synchrotrons Utilization Division, Raja Ramanna Centre for Advanced Technology, Indore 452013, India*

[2]*Department of Applied Physics, University of Tokyo, Hongo 7-3-1, Tokyo 113-8656, Japan*

(Received 17 November 2014; revised manuscript received 8 January 2015; published 23 February 2015)

Recently, phosphorene, a monolayer honeycomb structure of black phosphorus, was experimentally manufactured and has attracted rapidly growing interest. Motivated by phosphorene, here we investigate the stability and electronic properties of the honeycomb structure of the arsenic system based on first-principles calculations. Two types of honeycomb structures, buckled and puckered, are found to be stable. We call them arsenenes, as in the case of phosphorene. We find that both buckled and puckered arsenenes possess indirect gaps. We show that the band gap of puckered and buckled arsenenes can be tuned by applying strain. The gap closing occurs at 6% strain for puckered arsenene, where the bond angles between the nearest neighbors become nearly equal. An indirect-to-direct gap transition occurs by applying strain. Specifically, 1% strain is enough to transform puckered arsenene into a direct-gap semiconductor. We note that a bulk form of arsenic called gray arsenic exists which can be used as a precursor for buckled arsenene. Our results will pave the way for applications to light-emitting diodes and solar cells.

DOI: 10.1103/PhysRevB.91.085423 PACS number(s): 68.65.−k, 61.46.−w, 81.07.−b, 31.15.E−

I. INTRODUCTION

Graphene, a planar honeycomb monolayer of carbon atoms, is one of the most fascinating materials [1,2]. It has high mobility, heat conductance, and mechanical strength. However, it lacks an intrinsic band gap, which makes electronic applications of graphene difficult. The finding of graphene excited the material search for other monolayer honeycomb systems with intrinsic gaps. Recently, honeycomb structures of the carbon group have attracted much attention: silicene, germanene, and stanene [3]. The geometric structures of these systems are buckled due to the hybridization of sp^2 and sp^3 orbitals. Accordingly, we can control the band gap by applying a perpendicular electric field [4–6]. These are topological insulators owing to spin-orbit interactions [7]. Although silicene and germanene have already been manufactured on substrates [8–10], their free-standing samples are not yet available, which makes experiments to reveal their exciting properties difficult. Phosphorene, a monolayer of black phosphorus, was recently manufactured by exfoliating black phosphorus [11–16]. It has already been shown that it acts as a field-effect transistor [11]. The experimental success caused a recent flourish of studies on phosphorene [17–23]. The structure is puckered, which is different from planar graphene and buckled silicene. Furthermore, buckled phosphorene, called blue phosphorene, was shown to be stable using first-principles calculations [24].

In this paper, motivated by recent studies on phosphorene, we have investigated the stability and electronic properties of arsenene, which is a honeycomb monolayer of arsenic, by employing electronic structure calculations based on density functional theory (DFT). First, we show that two types of honeycomb structures, namely, buckled and puckered, are stable by investigating the phonon spectrum and cohesive energy. Our calculations show that buckled arsenene is slightly more stable than puckered arsenene. Although both systems possess indirect band gaps, it is possible to make a transition from an indirect to a direct band gap by applying strain or an external electric field. Puckered arsenene is transformed into a direct-gap semiconductor by applying only 1% strain, and the gap nearly closes at 6% strain. The band gap of buckled arsenene can be tuned by the electric field, while the band gap change is negligible for puckered arsenene.

This paper is organized in the following manner. In the next section, we describe the computational details employed in the present work. Section III contains the results and discussion, and then in Sec. IV, we summarize our results.

II. COMPUTATIONAL DETAILS

We use the QUANTUM ESPRESSO package [25] to perform fully self-consistent DFT [26] calculations by solving the standard Kohn-Sham (KS) equations. For the exchange-correlation (XC) potential, the generalized gradient approximation given by Perdew, Burke, and Ernzerhof (PBE) [27] has been utilized. We use the Vanderbilt ultrasoft pseudopotential [28] for an As atom that includes the scalar-relativistic effect [29]. Kinetic-energy cutoffs of 30 and 120 Ry have been used for electronic wave functions and charge densities, respectively. We adopt the Monkhorst-Pack scheme for k-point sampling of Brillouin zone integrations with $31 \times 31 \times 1$ and $31 \times 21 \times 1$ for the buckled/planar and puckered systems, respectively. The convergence criteria for energy in SCF cycles is chosen to be 10^{-10} Ry. The geometric structures are optimized by minimizing the forces on individual atoms with the criterion that the total force on each atom is below 10^{-3} Ry/bohr. In order to mimic the two-dimensional system, we employ a supercell geometry with a vacuum of about 18 Å in the z direction (the direction perpendicular to the plane of arsenene) so that the interaction between two adjacent unit cells in the periodic arrangement is negligible. The geometric structures are drawn using XCRYSDEN software [30]

*ckamal@rrcat.gov.in

†ezawa@ap.t.u-tokyo.ac.jp

III. RESULTS AND DISCUSSION

A. Stability of arsenene

Graphene forms a planar honeycomb structure since it exhibits purely sp^2 hybridization. On the other hand, other elemental honeycomb systems that have been found so far are not planar and form either a buckled or puckered structure. For example, a honeycomb structure of a group-IV element such as silicene, germanene, and stanene forms a buckled structure. Additionally, phosphorene made of phosphorus belonging to group V is known experimentally to have a puckered structure. It has theoretically been shown that there is also a buckled structure of phosphorene called blue phosphorene [24]. These observations make it important to study if there is a stable honeycomb structure made of arsenic, another group-V element. For this purpose, we choose three different possible honeycomb geometric structures, namely, (i) puckered, (ii) planar, and (iii) buckled, for arsenene. We show the optimized geometric structures for these three cases in Figs. 1(a)–1(c). The results of optimized geometric structures are also summarized in Table I. We find that the bond lengths of these two-dimensional structures are less than that in bulk arsenic. The puckered angle of arsenene is 100.80°, which is slightly smaller than that of phosphorene 103.69° [13]. In the case of the buckled structure, the buckling height and angle are found to be 1.388 Å and 92.22°, respectively.

In order to study the stability of arsenene, we have carried out the cohesive-energy calculations as well as phonon-dispersion calculations for the above-mentioned three possible structures. Cohesive energies are −2.952, −2.391, and −2.989 eV/atom for puckered, planar, and buckled arsenenes, respectively. Among the three two-dimensional structures, buckled arsenene is the minimum-energy configuration. However, the cohesive-energy difference between the buckled and puckered systems is very small, and it is comparable to the thermal energy at room temperature. On the other hand, the cohesive energy of the planar structure is about 400 meV less than those of the other two structures. In order to compare the stability of arsenene, we have also carried out the calculation of the stability on bulk gray arsenic. The buckling height is 1.291 Å, and the angle is 96.72° for bulk gray arsenic. These values are very close to those of buckled arsenene. It is very important to note that the cohesive energies of the puckered and buckled structures are quite close to that of bulk arsenic (−2.986 eV/atom; see Table I). Hence, the growth of these two stable structures of arsenene is energetically favorable.

Graphene is manufactured by exfoliating graphite. Recently, phosphorene has also been manufactured by exfoliating black phosphorus. We wish to emphasize that a bulk form of arsenic called gray arsenic exists [31,32] that containing layers of buckled arsenene. Thus, it is possible to obtain buckled arsenene by exfoliating gray arsenic, as in the cases of graphene and phosphorene. Since the cohesive energy of puckered arsenene is very close to those of both buckled arsenene and bulk gray arsenic, the possibility of manufacturing puckered arsenene experimentally also exists. Our results will motivate experimentalists to grow arsenene.

Furthermore, we have performed the phonon-dispersion calculations for these three systems. The results of phonon dispersion along the high symmetric points in the Brillouin zone [see Figs. 1(d)–1(f)] for these three systems are given in Figs. 1(g)–1(i). From the phonon spectrum, it is possible to compare the stability and structural rigidity of these systems. Puckered arsenene is globally stable since the global energy minimum exists, and the phonon dispersion is completely positive and linear around the Γ point. In the case of buckled arsenene, all modes contain positive frequencies except the transverse acoustic mode near the Γ point. This mode gets negative frequencies due to the softening of phonons, and a similar situation has been reported in the literature for buckled germanene [33], for which a strong dependence of the frequency of this mode on the computational parameters has also been observed. On the other hand, planar arsenene is not stable since it possesses a few modes with imaginary frequencies in a large region of the Brillouin zone, which corresponds to negative values in Fig. 1(h). From the detailed analysis of the phonon spectra, we infer that, of the 12 phonon modes of puckered arsenene, half of them are Raman active, and they are 97, 112, 215, 217, 247, and 253 cm^{-1} with the C_{2h} point-group symmetry at the Γ point. In the case of buckled arsenene, all three modes of the optical branch are Raman active. They are 236 cm^{-1} (doubly degenerate) and 305 cm^{-1} with the D_{3d} point-group symmetry at the Γ point.

It should be noted that most of the recently discovered two-dimensional systems like phosphorene and silicene show structural degradation in the ambient environment. Thus, although our theoretical calculations predict that pure buckled and puckered arsenenes are stable in terms of energetics and structural rigidity, the situation may change when the systems are kept in the ambient environment. Further investigations are required to understand their stability in the ambient environment.

B. Band structures

We show the electronic band structures for puckered, planar, and buckled arsenenes in Figs. 1(j)–1(l). In order to understand the contribution of different orbitals to the electronic states, we carry out the calculations of total (DOS) and partial (PDOS) densities of states for these three structures, and the results are summarized in Figs. 1(m)–1(o). We find that planar arsenene is metallic. We shall not continue to discuss any of its properties since it does not correspond to a stable structure. Both puckered and buckled arsenenes are semiconductors with indirect band gaps of 0.831 and 1.635 eV, respectively. It is observed from the PDOS of buckled and puckered arsenenes that the states near the Fermi level have contributions from both S and P orbitals. However, the contributions from the P orbitals to the total DOS are much higher than that from S orbitals. The fact that the P orbitals are dominant is a common feature of monolayer honeycomb systems such as silicene and phosphorene, where sp^2-like bonds form a nonplanar honeycomb structure. An indirect band gap in buckled arsenene resembles that of buckled (blue) phosphorene [24]. However, there are certain differences in the band structures of buckled phosphorene and arsenene. In the case of buckled arsenene [see Fig. 1(i)], the valence-band maximum lies at the Γ point, and the conduction-band minimum occurs along the Γ-M direction, whereas in buckled phosphorene, neither the conduction-band minimum nor the valence-band maximum lies at the high-symmetry k

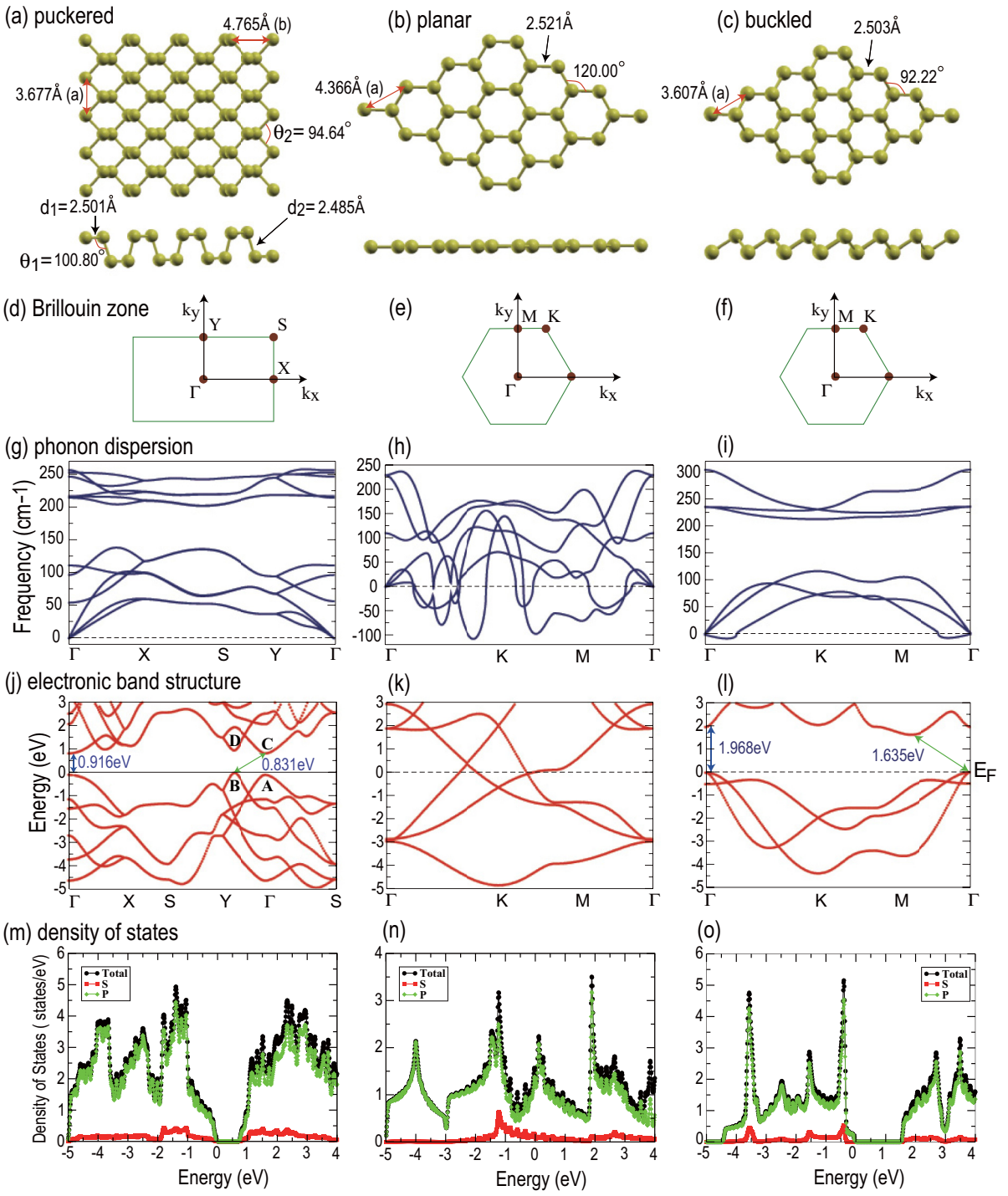

FIG. 1. (Color online) Optimized geometric structures, phonon dispersion curves, electronic band structure, and density of states of puckered, planar, and buckled arsenenes. Fully optimized structure of (a) puckered (b) planar, and (c) buckled arsenene. The length of the red arrow indicates the lattice constant. Brillouin zone of (d) puckered (e) planar, and (f) buckled arsenenes. The Brillouin zone of puckered arsenene is rectangular, while those of planer and buckled arsenene are hexagonal. We mark the high symmetric points. (g) (h),(i): Phonon dispersion curves for (g) puckered (h) planar, and (i) buckled arsenenes. Puckered arsenene is globally stable since the global minimum exists at the Γ point. Planar arsenene is unstable since it possesses a few modes with negative frequency. In buckled arsenene, all the modes contain positive values of frequency except the transverse acoustic mode near the Γ point. Electronic band structure of (j) puckered, (k) planar, and (l) buckled arsenenes. The indirect band gap (direct band gap at Γ) is indicated by the green (blue) arrow. Puckered and buckled arsenenes are indirect semiconductors, while planar arsenene is a metal. Total and partial densities of states of (m) puckered, (n) planar, and (o) buckled arsenene. The *P* orbitals are dominant for all structures.

TABLE I. The results for optimized geometries of arsenene obtained using DFT with the PBE exchange-correlation functional.

Structure	Space group	Cohesive energy (eV/atom)	Lattice constants (Å)		Bond length (Å)	Bond angle (deg)
			a	**b** or **c**		
Puckered	$Pmna$	−2.952	3.677	4.765 (**b**)	2.501, 2.485	100.80, 94.64
Planar	$P6/mmm$	−2.391	4.366		2.521	120.00
Buckled	$P3m1$	−2.989	3.607		2.503	92.22
Bulk	$R-3m$	−2.986	3.820 (3.7598) [31]	10.752 (**c**) (10.5475) [31]	2.556	96.72

points in the Brillouin zone [24]. Moreover, the difference between the indirect band gap (1.635 eV) and the direct gap (1.968 eV) at the Γ point is quite large (0.333 eV) for buckled arsenene.

On the other hand, the indirect-gap semiconducting character of puckered arsenene is distinctly different from the direct band gap of puckered phosphorene. We note that, in puckered arsenene, two separate valence- and conduction-band edges exist near the Fermi energy. The competition between the energies of these edges crucially determines the nature of the semiconducting behavior. In puckered arsenene, the maximum of the valence band and the minimum of the conduction band occur along the Γ-Y direction and at the Γ point, respectively. This causes puckered arsenene to behave as an indirect-gap semiconductor. This is in contrast to the direct gap present at the Γ point in puckered phosphorene [20]. Moreover, we clearly see from Fig. 1(j) that the difference in energies between two valence-band edges near the Fermi level is very small (only 85 meV) compared with that in puckered phosphorene (more than 500 meV) [20]. The difference is of the order of thermal energy at room temperature. In the next section, we analyze the effect of mechanical strain on the electronic structures of puckered arsenene and show that it is possible to transform puckered arsenene to a direct-gap semiconductor by applying strain.

C. Strain-induced band gap change

1. Puckered arsenene

Applying mechanical strain to the sample is a powerful method for modulating the electronic properties of

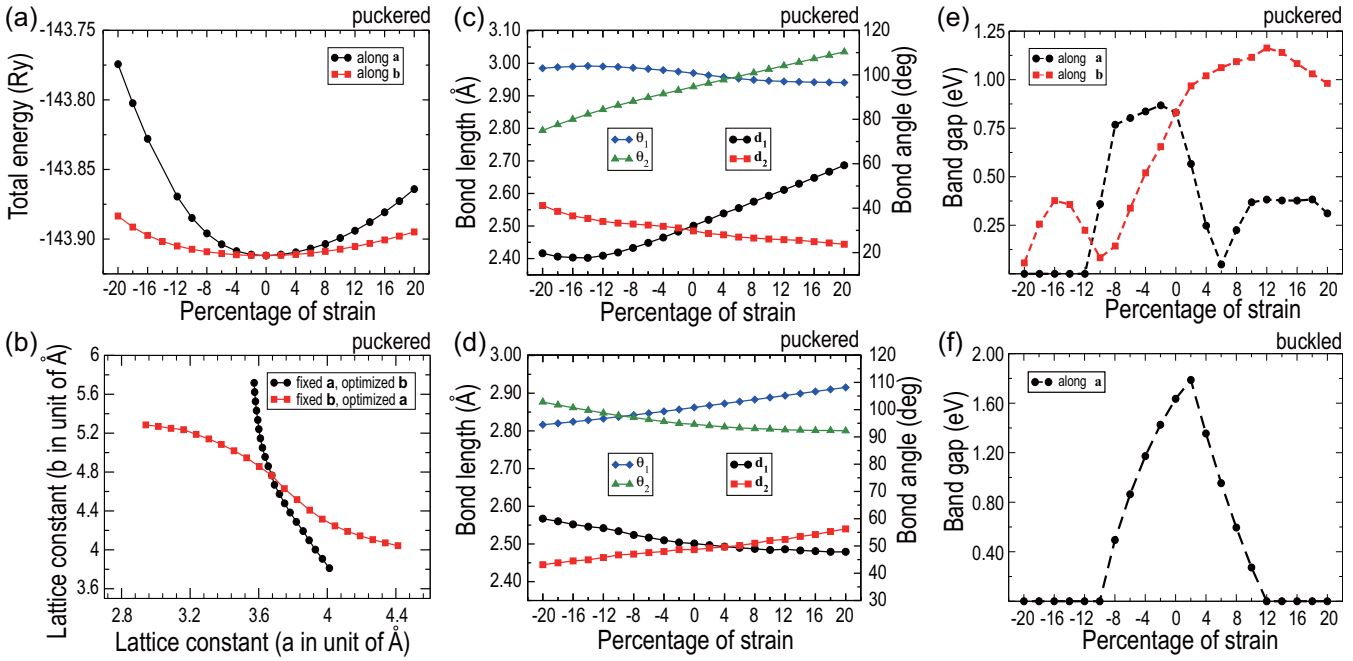

FIG. 2. (Color online) Effect of strain on energy, geometric structure, and band structure. (a) Variation of the total energy with strain along lattice vectors **a** and **b** for puckered arsenene. The total energy is parabolic, where the bottom is at 0% strain. The total energy with strain along lattice vectors **a** is higher than that along lattice vectors **b**. (b) The intersection of two curves represents the globally optimized lattice constants **a** and **b**. Black circles (red squares) show the optimized lattice constant **b** (**a**) by fixing lattice constant **a** (**b**). (c) and (d) Variation of bond lengths and bond angles with strain along lattice vectors **a** and **b**. Around the equilibrium structure, the bond length and angle vary linearly with strain. Angles θ_1 and θ_2 become the same at 6% (−10%) strain along lattice vector **a** (**b**), where the band gap nearly closes. See Figure 3. (e) The band gap for puckered arsenene. The band gap reaches the minimum at 6% (−10%) strain along lattice vector **a** (**b**), while it is maximum at −2% (12%) strain along lattice vector **a** (**b**). The band gap is zero beyond −12% strain along lattice vector **a**, where the system becomes metallic. (f) The band gap for buckled arsenene. The band gap attains the maximum value at 2% strain. The system becomes metallic beyond 12% and −10% strain due to the overlap between the valence and conduction bands.

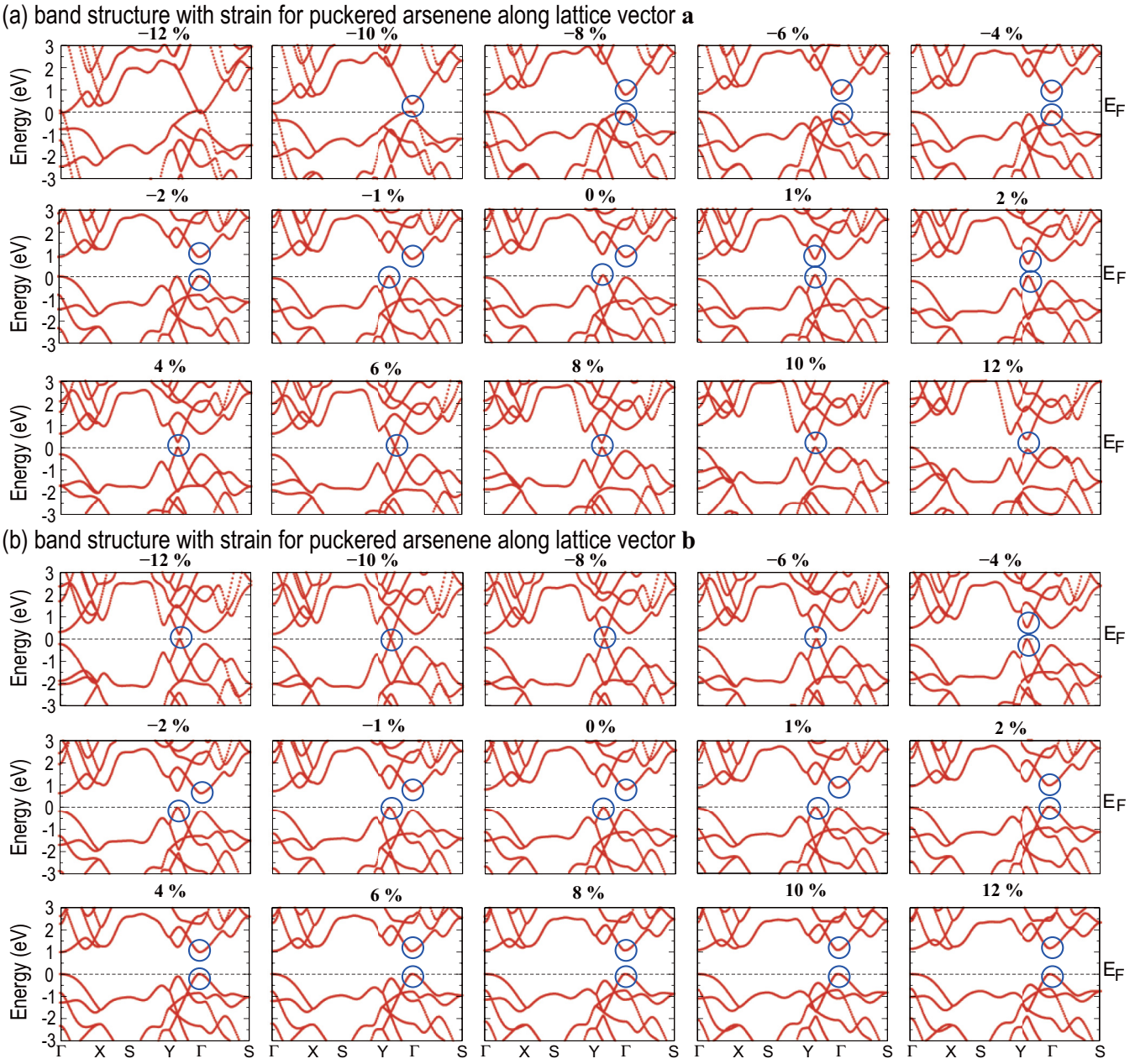

FIG. 3. (Color online) Variation of electronic band structures with strain along lattice vectors **a** and **b**. (a) The band gap nearly closes at 6% strain. The system is metallic beyond −12% strain. The indirect-to-direct gap transition occurs at 1% and −2% strain. (b) The band gap nearly closes at −10% strain. The indirect-to-direct gap transition occurs at 2% and −4% strain. The blue circles indicate the lowest conduction-band and highest valence-band edges.

materials. There are several reports which suggest that the band structure of phosphorene can be modified by applying strain [12,17,19,20]. In the present case, we study the evolution of the electronic properties of puckered arsenene when it is subjected to mechanical strain, both tensile and compressive, along two separate lattice vectors, **a** and **b**. The application of mechanical strain is simulated by freezing one of the lattice constants, which is different from the optimized value, and then varying the other lattice constant as well as the internal degrees of freedom of each atom during the geometric optimization. Thus, the effect of strain is translated into the difference ($\Delta\mathbf{a}$ or $\Delta\mathbf{b}$) between the frozen and globally optimized lattice constants. For this purpose, we choose the range of $\Delta\mathbf{a}$ and $\Delta\mathbf{b}$ from −20% to 20% of the optimized lattice constants with spacing of 2%. We assign the positive and negative values for compressive and tensile strains, respectively. First, we evaluate the total energy of the puckered structure when strain is applied, and the results are shown in Fig. 2(a). Puckered and buckled arsenenes are energetically stable under very strong compressive and tensile strains. The total energy with strain along the b axis is lower than that with strain along the a axis. It is natural that we can easily compress or expand the puckered structure along the b axis by changing the puckered angle θ_1. On the other hand, the structure is planar along the a axis,

which makes it difficult to change the structure along the a axis. In Fig. 2(b), we present the optimized lattice constants a and b during the compressive and tensile strains. For strain along the a axis, we first fix the lattice constant a and then optimize the lattice constant b. Similarly, we perform the optimization of the lattice constant a with a fixed value of the lattice constant b for the strain along the b axis.

We also carry out a detailed analysis of the geometric structure of strained puckered arsenene. The results of this analysis are plotted in Figs. 2(c) and 2(d) for strains along the a and b axes, respectively. In the case of the puckered structure, there are two types of bond lengths (d_1 and d_2) and bond angles (θ_1 and θ_2). Around the optimized structures, both the bond lengths and the bond angles vary linearly with the amount of strain. An increase in one of the bond lengths (or angles) results in a decrease in the other bond length (or angle). This is due to the fact that the compression in one of the lattice directions leads to the relaxation of atoms in the other direction.

Now, we discuss the modulations in the band structures of puckered arsenene by applying strain along lattice vectors **a** [in Fig. 3(a)] and **b** [in Fig. 3(b)]. We first investigate the band structures with strain along the a axis. We find from Fig. 3(a) that there is an indirect-to-direct gap transition due to both compressive and tensile strains along the a axis. However, the locations of the direct band gap in the k vector for these two strains are different. In the case of compressive strain, the location of the direct band gap occurs at the Γ point, whereas for tensile strain, the direct band gap lies along the Γ-Y direction. It is remarkable that the system remains a direct-gap semiconductor for a wide range values of strains from -10% to 10% except in the vicinity of no strain. This is a significantly important result from an application point of view since it can accommodate possible structural deformations, which may arise during growth or device manufacturing, while retaining its direct-gap semiconducting behavior.

Other important observations from Fig. 3(a) are the gap closing and the emergence of a linear dispersion around the Fermi energy along the Γ-Y direction for a tensile strain of 6%. In this situation, the system possesses a strong anisotropy in the electronic band structure: Dirac-like (linear) dispersion along the Γ-Y direction and Schrödinger-like (parabolic) dispersion in other direction. Thus, the point in E-k diagram where the gap closes is a semi-Dirac point. In Figs. 2(e) and 2(f), we plot the variation of the band gap as a function of strain. We observe that the band gap of puckered arsenene becomes smaller when we apply tensile strain along the a axis. The gap nearly closes at 6% strain, and then the band gap increases. On the other hand, for compressive strain along the a axis, the band gap initially decreases and becomes metallic around -12% due to the significant overlap between the conduction and valence bands.

Next, we investigate the band structures with strain along the b axis. We find from Fig. 3(b) that the application of strain along the b axis produces effects nearly the same as those in the case of strain along the a axis, but in the opposite direction. This is natural because if we apply tensile strain along the b axis, the system is elongated along the b axis and shortened along the a axis. This kind of deformation also

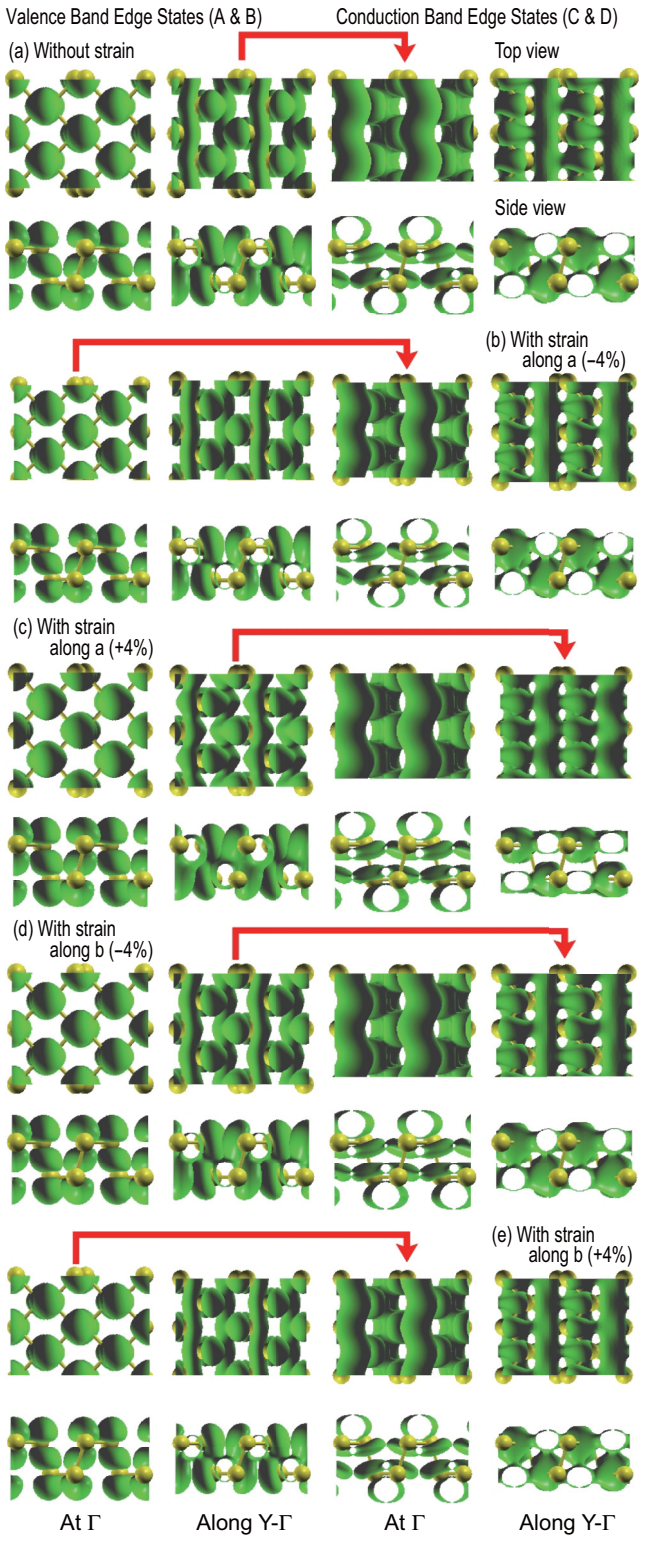

FIG. 4. (Color online) Charge density distribution of the two valence (A and B) and two conduction-band (C and D) edge states, near Fermi level, for puckered arsenene. (a) Without strain. (b) With -4% strain along **a**. (c) With $+4\%$ strain along **a**. (d) With -4% strain along **b**. (e) With $+4\%$ strain along **b**. The red arrows indicate the minimum-energy transition between these states.

occurs when we apply compressive strain along the a axis. Here we also observe an indirect-to-direct band gap transition due to strain. Furthermore, the band gap of puckered arsenene becomes smaller, and then the gap nearly closes at -10% due to compressive strain. We note that the band structure of puckered arsenene with -10% compressive strain along the b axis is almost the same as that with 6% tensile strain along the a axis.

We find a strong correlation between the emergence of a linear dispersion in the band structure and the geometric structure of puckered arsenene. A closer look at Figs. 2(c) and 2(d) reveals that when the bond angles between the nearest neighbors become nearly equal ($\theta_1 \approx \theta_2$), the system possesses a nearly linear dispersion in the electronic band structure. This can be understood as follows. When the two angles become equal, each arsenic atom is surrounded by three nearest neighbors with same angle. It makes the local environment more symmetric in spite of having nonhexagonal or nontrigonal crystal symmetries, which results in the gap closing with a nearly linear dispersion.

We have also calculated the charge density distribution of two valence-band and two conduction-band edge states which lie near the Fermi level [which are represented as A, B, C, and D in Fig. 1(j)] for puckered arsenene. The spatial distribution of charges corresponding to these four states, without and with strains, are plotted in Fig. 4. From Fig. 4(a), we have observed that valence state A at the Γ point is nearly localized, whereas valence state B, which lies along the Γ-Y direction, shows a delocalized distribution of charges along the lattice vector **a**. The two conduction-band edge states, C and D, also possess nearly the same delocalized distribution of charges along the a axis. We have observed that there are very small changes in the spatial distribution of charges when the system is subjected to mechanical strains. For example, in Figs. 4(b)–4(e), we have plotted the charge density for puckered arsenene with $\pm 4\%$ of strains along both the a and b axes. However, these small changes are enough to alter the nature of the electronic transition from indirect to direct since the energy difference between these two valence-band and two conduction-band edge states is also small.

The indirect-to-direct gap transition as a result of strain can be interpreted in the same manner as the transition in phosphorene [20]. The energy shift of the band edge can be understood in terms of the bonding and antibonding states. As shown in Fig. 8(h) of the work on phosphorene [20], the energy shifts of the bonding and antibonding states are opposite, while that of the nonbonding states does not shift. The wave functions of states A, B, and C in our work correspond well to those of Ref. [20]. As a result, the band edges at A, B, and C shift in a way similar to those of phosphorene. The difference between phosphorene and arsenene is the energy of the band edges, which depends on the chemical characters. As a result, the indirect-to-direct gap transition occurs in arsenene, while the direct-to-indirect gap transition occurs in phosphorene.

Our DFT-based calculations predict that it is possible to produce the following modifications in puckered arsenene by applying mechanical strains: (i) indirect-to-direct band gap transition, (ii) semiconductor-semimetal transition, and (iii) semiconductor-metal transition. Furthermore, the band gap of puckered arsenene can also be tuned over a wide range. These results suggest that puckered arsenene can be chosen as one of the promising nanomaterials for several applications, including optoelectronic devices.

2. *Buckled arsenene*

Like we did for puckered arsenene, we have also performed studies on the effect of strain on the properties of buckled arsenene. In this case, we apply compressive and tensile strains symmetrically along its primitive lattice vectors. Then, the

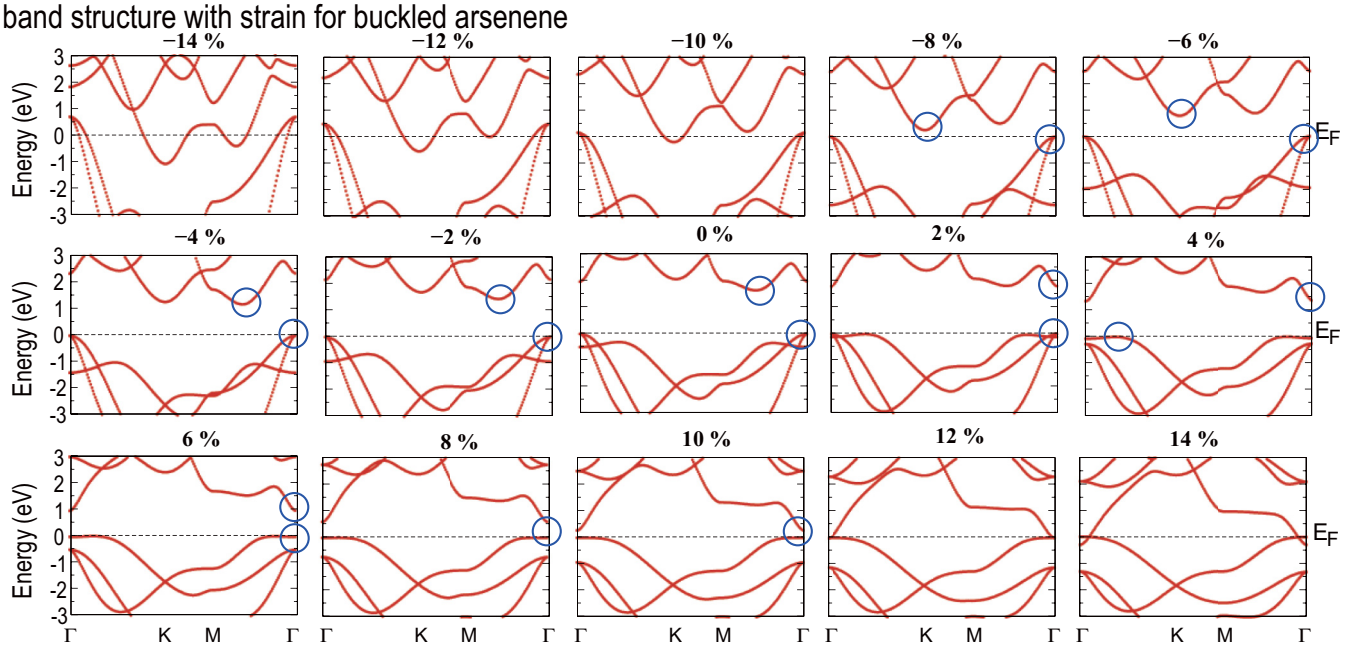

FIG. 5. (Color online) Variation of electronic band structures as a function of strain for buckled arsenene. The system becomes metallic beyond 12% and -10% strain. The blue circles indicate the lowest conduction-band and highest valence-band edges

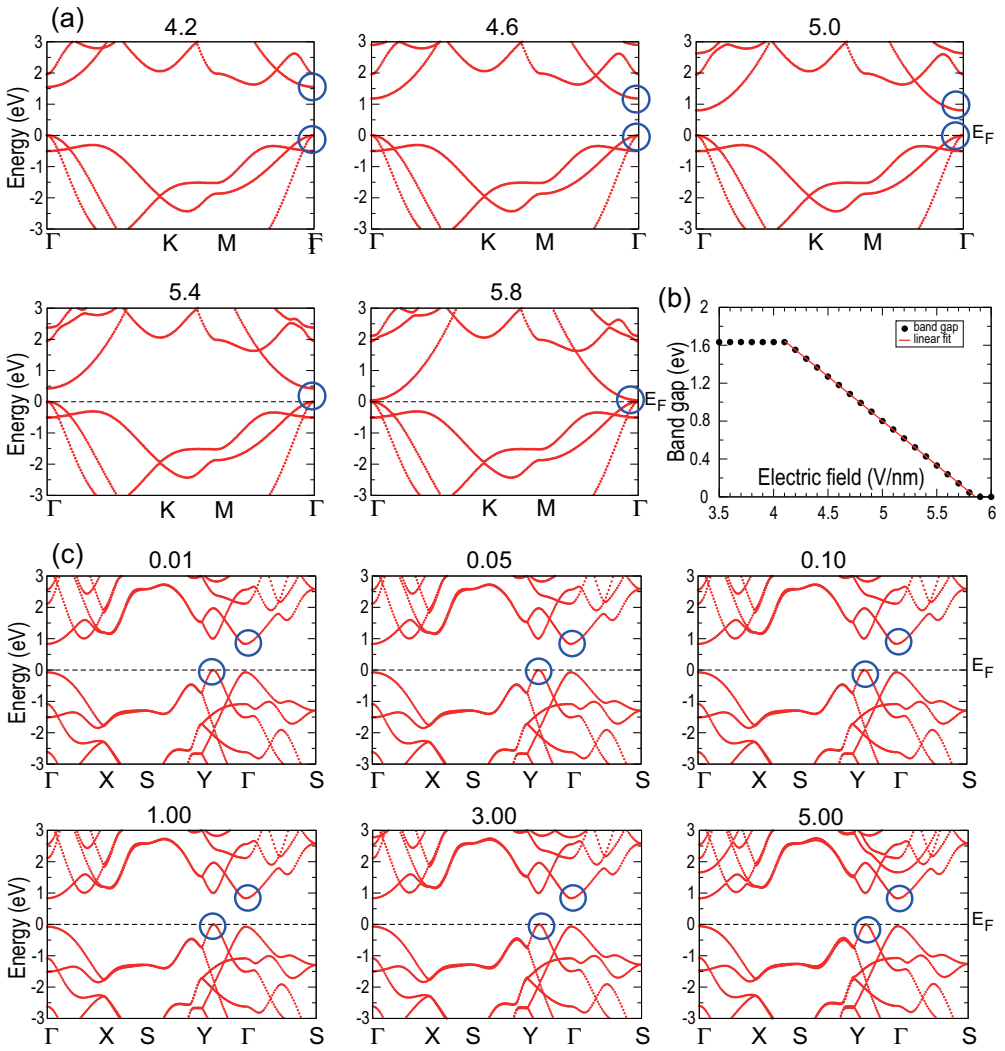

FIG. 6. (Color online) Variation of electronic band structures with the transverse static electric field for buckled and puckered arsenenes. (a) Buckled arsenene. The value above the subfigure represents the strength of the transverse electric field in units of V/nm. The system becomes a direct-gap semiconductor beyond 4.2 V/nm and then becomes a metal beyond 5.8 V/nm due to the overlap between the valence and conduction bands. (b) The evolution of the band gap with the strength of electric field. The band gap is constant below 4.2 V/nm, where the system is an indirect-gap semiconductor. The band gap linearly decreases between 4.2 and 5.8 V/nm. (c) Puckered arsenene. There is no change in the electronic structures, near the Fermi level, of puckered arsenene when it is subjected to electric field strengths up to 5.0 V/nm. The blue circles indicate the lowest conduction-band and highest valence-band edges.

amount of strain is directly quantified in terms of change in the lattice constant Δa. Around the equilibrium geometric structure, the total energy of the system shows a parabolic behavior, while the bond length and angle show nearly linear variations.

The band structure found by varying strain is shown in Fig. 5. Buckled arsenene mostly remains an indirect-gap semiconductor for both compressive and tensile strains. The variation in the indirect band gap with strain is plotted in Fig. 2(f). The band gap slowly decreases with the increase in either compressive or tensile strain. Then, the system goes from semiconducting to metallic for strains beyond -10% and 12%.

D. Electric-field-induced band gap change

Applying a perpendicular electric field to a buckled honeycomb structure such as silicene is shown to be an effective way to directly control the band gap [4–6]. In the buckled honeycomb structure, a separation exists between the A and B sublattices. Then, the perpendicular electric field acts as the staggered potential for the honeycomb system. It is an interesting problem to investigate how the band structure of buckled arsenene is modified under an electric field. We have performed calculations with the strength of the perpendicular electric field ranging from 0.0 to 6.0 V/nm. It is found that there is no change in the band gap of buckled arsenene for an electric field strength up to 4.2 V/nm. The resultant band structures for some of the field strengths from 4.2 to 5.8 V/nm are shown in Fig. 6. As discussed earlier, without an electric field, buckled arsenene is an indirect semiconductor. There is an indirect-to-direct gap transition at 4.2 V/nm. We show the band gap as a function of the electric field in Fig. 6(b). For 4.1 V/nm $< E <$ 5.8 V/nm, the band gap decreases linearly with the strength of the electric field. Based on the linear fit,

we find that the band gap closes at the critical electric field $E = 5.856$ V/nm. Above the critical field, the conduction band starts to overlap with the valence band and makes the system metallic. We note that the electric field required for the indirect-to-direct transition is quite high, which makes experiments difficult.

Similarly, we have also performed band structure calculations for puckered arsenene when it is under the influence of an electric field. It is observed from Fig. 6(c) that there is no change in the electronic structures near the Fermi level for strengths of the electric field up to 5.0 V/nm. The fact that the band structure of puckered arsenene does not change under an electric field can be understood as follows. In the puckered structure, the numbers of A and B sites are the same in both higher and lower layers. This is in contrast to the case of the buckled structure, where all A sites are in the higher layer while all B sites are in the lower layer. As a result, the electric field does not act as the staggered potential in puckered arsenene, which results in the absence of the band structure modification by the electric field.

IV. SUMMARY

We predict that the puckered and buckled structures of arsenene are stable from both the energetics and structural-rigidity points of view based on the DFT calculations. Results of cohesive energy calculations show that the cohesive energies of both puckered and buckled arsenenes are very close to that of bulk gray arsenic and there is a possibility of manufacturing arsenene experimentally. These two structures are semiconductors with indirect band gaps. Interestingly, puckered arsenene goes from an indirect-gap to direct-gap semiconductor due to structural deformation along any of its lattice vectors. Furthermore, the onset of this transition occurs at a very small amount of lattice deformation (1%). It is also possible to tune the band gaps of this system over wide range while keeping its direct-gap semiconducting behavior by applying compressive and tensile strains. Another important observation is the presence of the Dirac-like dispersion along the Γ-Y direction when the system is subjected to either compressive or tensile strain along its lattice vectors. For larger compressive strain, the system is transformed from a semiconductor to a metal due to a strong overlap of orbitals corresponding to the valence and conduction bands. Experimentally, it is possible to induce a strain using the beam-bending apparatus [34], scanning tunnel microscope tips for tensile strain [35], and substrates, and hence, the results predicted can be verified once arsenene is grown on a substrate or exfoliated from its bulk counterpart. The indirect-to-direct band gap transition found in puckered arsenene may open up the possibility of using this two-dimensional system in several optoelectronic devices such as light-emitting diodes and solar cells.

ACKNOWLEDGMENTS

C.K. thanks Dr. G. S. Lodha and Dr. P. D. Gupta for support and encouragement. C.K. also thank the Scientific Computing Group, RRCAT, for its support. M.E. acknowledges the support from the Grants-in-Aid for MEXT KAKENHI (Grant No. 25400317). C.K. and M.E. are very grateful to Dr. A. Chakrabarti and Prof. N. Nagaosa for many helpful discussions on the subject.

[1] A. H. Castro Neto, F. Guinea, N. M. R. Peres, K. S. Novoselov, and A. K. Geim, Rev. Mod. Phys. **81**, 109 (2009).
[2] M. I. Katsnelson, *Graphene: Carbon in Two Dimensions* (Cambridge University Press, Cambridge, 2012).
[3] C. C. Liu, H. Jiang, and Y. Yao, Phys. Rev. B **84**, 195430 (2011).
[4] N. D. Drummond, V. Zolyomi, and V. I. Fal'ko, Phys. Rev. B **85**, 075423 (2012).
[5] M. Ezawa, New J. Phys. **14**, 033003 (2012).
[6] C. Kamal, A. Banerjee, and A. Chakrabarti, in Graphene Science Handbook: Size-Dependent Properties, Chapter 40: Properties of Two-Dimensional Silicon versus Carbon Systems, edited by M. Aliofkhazraei, N. Ali, W. I. Milne, C. Z. Ozkan, S. Mitura, and J. L. Gervasoni (CRC Press, Taylor & Francis Group) (in press).
[7] C. C. Liu, W. Feng, and Y. Yao, Phys. Rev. Lett. **107**, 076802 (2011).
[8] P. Vogt, P. De Padova, C. Quaresima, J. Avila, E. Frantzeskakis, M. C. Asensio, A. Resta, B. Ealet, and G. Le Lay, Phys. Rev. Lett. **108**, 155501 (2012).
[9] C.-L. Lin, R. Arafune, K. Kawahara, N. Tsukahara, E. Minamitani, Y. Kim, N. Takagi, and M. Kawai, Appl. Phys. Express **5**, 045802 (2012).
[10] A. Fleurence, R. Friedlein, T. Ozaki, H. Kawai, Y. Wang, and Y. Yamada-Takamura, Phys. Rev. Lett. **108**, 245501 (2012).
[11] L. Li, Y. Yu, G. J. Ye, Q. Ge, X. Ou, H. Wu, D. Feng, X. H. Chen, and Y. Zhang, Nat. Nanotechnol. **9**, 372 (2014).
[12] H. Liu, A. T. Neal, Z. Zhu, X. Xu, D. Tomanek, and P. D. Ye, ACS Nano **8**, 4033 (2014).
[13] A. Castellanos-Gomez *et al.*, 2D Mater. **1**, 025001 (2014).
[14] F. Xia, H. Wang, and Y. Jia, Nat. Commun. **5**, 4458 (2014).
[15] S. P. Koenig, R. A. Doganov, H. Schmidt, A. H. Castro Neto, and B. Özyilmaz, Appl. Phys. Lett. **104**, 103106 (2014).
[16] M. Buscema *et al.*, Nat. Commun. **5**, 4651 (2014).
[17] A. S. Rodin, A. Carvalho, and A. H. Castro Neto, Phys. Rev. Lett. **112**, 176801 (2014).
[18] E. S. Reich, Nature (London) **506**, 19 (2014).
[19] R. Fei and L. Yang, Nano Lett. **14**, 2884 (2014).
[20] X. Peng, Q. Wei, and A. Copple, Phys. Rev. B **90**, 085402 (2014).
[21] Q. Wei and X. Peng, Appl. Phys. Lett. **104**, 251915 (2014).
[22] R. Fei and L. Yang, Appl. Phys. Lett. **105**, 083120 (2014).
[23] J. Qiao, X. Kong, Z.-X. Hu, F. Yang, and W. Ji, Nat. Commun. **5**, 4475 (2014).
[24] Z. Zhu and D. Tomanek, Phys. Rev. Lett. **112**, 176802 (2014).
[25] P. Giannozzi *et al.*, J. Phys. Condens. Matter **21**, 395502 (2009).
[26] P. Hohenberg and W. Kohn, Phys. Rev. **136**, B864 (1964); W. Kohn and L. J. Sham, *ibid.* **140**, A1133 (1965).
[27] J. P. Perdew, K. Burke, and M. Ernzerhof, Phys. Rev. Lett. **77**, 3865 (1996).

[28] D. Vanderbilt, Phys. Rev. B **41**, 7892 (1990).
[29] QUANTUM ESPRESSO, http://www.quantum-espresso.org/pseudopotentials.
[30] A. Kokalj, Comput. Mater. Sci. **28**, 155 (2003); XCRYSDEN code, http://www.xcrysden.org.
[31] D. Schiferl and C. S. Barrett, J. Appl. Crystallogr. **2**, 30 (1969).
[32] R. Boca *et al.*, Czech. J. Phys. **43**, 813 (1993).
[33] H. Sahin, S. Cahangirov, M. Topsakal, E. Bekaroglu, E. Akturk, R. T. Senger, and S. Ciraci, Phys. Rev. B **80**, 155453 (2009).
[34] H. J. Conley, B. Wang, J. I. Ziegler *et al.*, Nano Lett. **13**, 3626 (2013).
[35] C. Lee, X. Wei, J. W. Kysar, and J. Hone, Science **321**, 385 (2008).